AIAA JOURNAL SPECIAL SUPPLEMENT: CENTENNIAL OF POWERED FLIGHT
This paper reprinted from AIAA Journal, Vol. 9, No. 1, 1971, pp. 114–121

Calculation of Plane Steady Transonic Flows

EARLL M. MURMAN* AND JULIAN D. COLE†

Boeing Scientific Research Laboratories, Seattle, Wash.

Transonic small disturbance theory is used to solve for the flow past thin airfoils including cases with imbedded shock waves. The small disturbance equations and similarity rules are presented, and a boundary value problem is formulated for the case of a subsonic freestream Mach number. The governing transonic potential equation is a mixed (elliptic-hyperbolic) differential equation which is solved numerically using a newly developed mixed finite difference system. Separate difference formulas are used in the elliptic and hyperbolic regions to account properly for the local domain of dependence of the differential equation. An analytical solution derived for the far field is used as a boundary condition for the numerical solution. The difference equations are solved with a line relaxation algorithm. Shock waves, if any, and supersonic zones appear naturally during the iterative process. Results are presented for nonlifting circular arc airfoils and a shock free Nieuwland airfoil. Agreement with experiment for the circular arc airfoils, and exact theory for the Nieuwland airfoil is excellent.

Nomenclature

$\bar{C}_D$ = reduced drag coefficient = $(M_\infty^{2/3}/\delta^{5/3})C_D$
C_p = pressure coefficient = $(P - P_\infty)/\frac{1}{2}\rho_\infty U_\infty^2$
$\bar{C}_p$ = reduced pressure coefficient $(M_\infty/\delta)^{2/3}C_p = -2u$
$\mathfrak{D}$ = doublet strength
$F(x)$ = airfoil shape function
K = transonic similarity parameter = $(1 - M_\infty^2)/\delta^{2/3}$
K_s = transonic similarity parameter after Spreiter = $(1 - M_\infty^2)/(M_\infty^2\delta)^{2/3}$
M = mach number
P = pressure
p = perturbation pressure
Re_c = Reynolds number based on chord length
U = velocity
u,v = perturbation velocities in x and y directions, respectively
x,y = Cartesian coordinates
$\bar{y}$ = transonic lateral coordinate = $\delta^{1/3}y$
γ = ratio of specific heats
δ = thickness ratio of airfoil
θ = perturbation angle of flow
ρ = density
ϕ = perturbation potential
Φ_i = column vector of perturbation potentials

Subscripts

i,j = mesh point indices in x and y directions, respectively
s = evaluated on shock surface.
∞ = freestream condition

Superscript

$*$ = locally sonic conditions

I Introduction

PRESENT methods of computing transonic flowfields about high subsonic speed airplanes are based essentially on solution of incompressible flowfields with application of theoretical and empirical corrections for compressible effects. In this paper we present the theoretical background and computational procedure for the straightforward calculation of steady, inviscid transonic flow past airfoils, including the occurrence of shock waves. The ability to do this problem is essential for the computation of more complicated and realistic transonic problems involving boundary layers and three dimensionality. The methods developed have a basic mathematical interest since they provide a direct attack on problems involving equations of mixed (elliptic-hyperbolic) type.

A few theoretical and computational methods already exist for determining flowfields of airfoils flying in this speed range. We mention here only the most pertinent references. The principal theoretical approach is the hodograph method in which the equations for compressible potential flow are studied in the plane of the velocity components where they are linear. A wide variety of solutions can be constructed analytically, but the method has two drawbacks. First, the shape of the airfoil cannot be prescribed in advance, and second, shock waves cannot be treated. Further, the shape of the airfoil changes if either the freestream Mach number or thickness ratio is altered. Nevertheless these isolated solutions provide important check points. Nieuwland[1] has recently developed the method for mixed subsonic-supersonic, shock-free flows and obtained a series of interesting results. Another method has been presented by Korn[2] for calculating hodograph solutions based on complex characteristic finite difference methods. The technique shows promise for obtaining a wide variety of practical airfoil shapes with shock-free flows.

Among the methods for computing mixed flows with shock waves, only the work of Magnus and Yoshihara[3] appears promising. Their approach is to integrate the equations of unsteady compressible flow forward in time to approach a steady state. In doing this they rely on a body of knowledge already developed on the computational aspects of unsteady flow, including the treatment of shock waves. The results are encouraging, but the computations are lengthy, requiring about 2 hr on a CDC 6400. In addition, there are difficulties in applying the exact boundary conditions on the body surface. None of the other computational or theoretical methods which have been studied, such as integral equation methods, seem capable of computing flows in this speed range with sufficient accuracy.

For these reasons, we have tried to develop a new, simplified approach to the problem of computing mixed flowfields. Our method is based on the steady transonic small disturbance

Presented at the AIAA 8th Aerospace Sciences Meeting, New York, January 19–21, 1970; submitted February 13, 1970; revision received May 20, 1970. The authors wish to acknowledge the major programing contributions of J. Krupp, and the initial programing work of H. Mandt.

* Staff Scientist, Flight Sciences Laboratory. Member AIAA.
† Faculty Fellow, Flight Sciences Laboratory; presently at the School of Engineering and Applied Science, University of California at Los Angeles, Los Angeles, Calif.

equation which contains some sacrifice in accuracy but which allows a great simplification of both the equations and boundary conditions. An analytic representation is developed for the far field of an airfoil which is used as a boundary condition for the numerical computation. In the near field, the governing transonic potential equation is solved numerically using a newly developed mixed finite difference system. Separate difference formulas are used in the elliptic and hyperbolic regions to account properly for the local domain of dependence of the differential equation. The difference equations are then solved numerically by an iterative relaxation procedure. Shock waves, if any, appear naturally in the course of the solution. The method is accurate and converges well. Computations to date have been carried out for the nonlifting case although the ideas apply equally well for the lifting case. In Section II, the small-disturbance equations are presented. The far field solution is derived in Section III and some flowfield singularities are discussed. Section IV develops the numerical analysis, and some computed results are presented in Section V.

II Transonic Small Disturbance Theory

The transonic small disturbance equations are derived as a part of a systematic (asymptotic) expansion procedure applied to the exact equations of gas dynamics. The small parameter of the expansion procedure is taken to be the airfoil thickness ratio δ (see Fig. 1), and the flow is represented as small disturbances on a uniform stream. To obtain a meaningful first approximation equation the freestream Mach number M_∞ is considered to approach 1. In addition, the tendency of disturbances to spread laterally is taken into account by the use of a scaled coordinate $\tilde{y} = \delta^{1/3}y$. The limit process associated with the approximation is $\delta \to 0$; $K,x,\tilde{y}$ fixed where

$$K = (1 - M_\infty^2)/\delta^{2/3} = \text{transonic similarity parameter} \quad (1)$$

K is not defined uniquely but may be, for example, multiplied by functions like $g(M_\infty^2) = 0(1)$ where $g(1) = 1$. The orders of magnitude of the various perturbations, the similarity parameter, etc., are all suggested by the form of the shock wave relations or simple wave solutions. For details about the expansion procedure, including higher approximations, see Refs. 4 and 5. For simplicity, the expansion is presented here for the case of a symmetric airfoil (nonlifting) at zero angle of attack. The flow quantities have the representation

$$\begin{aligned} q_x/U &= 1 + \delta^{2/3}u + \ldots, \quad q_y/U = \delta v + \ldots \\ P/P_\infty &= 1 + \delta^{2/3}p + \ldots, \quad \rho/\rho_\infty = 1 + \delta^{2/3}\sigma + \ldots \end{aligned} \quad (2)$$

where $u = u(x,\tilde{y};K)$, $v = v(x,\tilde{y};K)$, etc. The order of the magnitude of q_y/U is fixed by the condition of tangent flow at the airfoil. Equations (2) are substituted into the inviscid equations of continuity, momentum balance, and entropy conservation (allowing jumps across shock waves), and the shock relations are taken into account. Various integrals are found and the following equations of motion result:

Bernoulli law
$$p = \gamma\sigma = -\gamma u \quad (3)$$

Mass-flux vector

$$\rho q_x/\rho_\infty U = 1 + \delta^{4/3}[Ku - (\gamma + 1)u^2/2] + \ldots$$
$$\rho q_y/\rho_\infty U = \delta v + \ldots \quad (4)$$

Transonic equations
$$[Ku - (\gamma + 1)u^2/2]_x + v_{\tilde{y}} = 0 \quad (5a)$$
$$v_x - u_{\tilde{y}} = 0 \quad (5b)$$

Equation (5a) is a transonic version of the continuity equation and Eq. (5b) shows that the flow to this order (and to second order also) is irrotational. Any shock waves which occur on slender airfoils in transonic flow are sufficiently weak

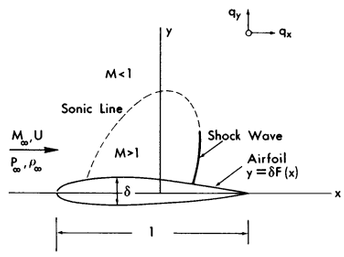

Fig. 1 Typical transonic flow past a slender airfoil.

to introduce negligible vorticity. A velocity potential can be introduced

$$u = \phi_x, \quad v = \phi_{\tilde{y}} \quad (6)$$

to obtain the benefits of computing a single function.

The system is replaced by the basic transonic equation

$$[K\phi_x - (\gamma + 1)\phi_x^2/2]_x + \phi_{\tilde{y}\tilde{y}} = 0 \quad (7)$$

or alternatively

$$[K - (\gamma + 1)\phi_x]\phi_{xx} + \phi_{\tilde{y}\tilde{y}} = 0 \quad (8)$$

Equation (8) has the form locally either of a wave equation (hyperbolic type), representing supersonic flow $\phi_x > K/(\gamma + +1)$, or of a Laplace equation (elliptic type), representing subsonic flow $\phi_x < K/(\gamma + 1)$. The essential role of the nonlinear term allows this transition. The local Mach lines (characteristics) have the slope

$$(d\tilde{y}/dx) = \pm[(\gamma + 1)\phi_x - K]^{-1/2} \quad (9)$$

The local flow angle is given by

$$\tan\vartheta = q_y/q_x = \delta v + \ldots = \delta\theta + \ldots \simeq \vartheta$$

The shock jump conditions must be added to the system Eqs. (5) or Eq. (8) to form a complete system. However, it turns out that the shock jump conditions are contained in Eqs. (5) [or in Eq. (8)] in the following sense. If these differential equations are integrated across a jump in (u,v), the correct shock relations, to this order, result. That is, Eqs. (5) are in conservation, or divergence form. The corresponding surface integral forms give the shock jumps

$$\begin{aligned} \langle Ku - (\gamma + 1)u^2/2\rangle(d\tilde{y})_s - \langle v\rangle(dx)_s &= 0 \\ \langle v\rangle(d\tilde{y})_s + \langle u\rangle(dx)_s &= 0 \end{aligned} \quad (10)$$

where $\langle\rangle$ denote a jump in the quantity across the shock and subscript s denotes an element in the shock surface.

The shock jump conditions Eq. (10) yield easily the shock polar representation

$$[K - (\gamma + 1)\bar{u}_s]\langle u\rangle^2 + \langle v\rangle^2 = 0 \quad (11)$$

where $\bar{u}_s = (u^{(2)} + u^{(1)})/2$ is the average of u across the shock. The shock wave angle in the $(x,\tilde{y})$ plane is measured by θ_s,

$$\theta_s = dx/d\tilde{y} = -\langle v\rangle/\langle u\rangle \quad (12)$$

For a normal shock, $\langle v\rangle = 0$ and Eq. (11) reduces to

$$\bar{u}_s = K/(\gamma + 1) \quad (13)$$

which is a transonic version of Prandtl's equation. Finally we note

$$\langle\phi\rangle = 0 \quad (14)$$

a condition which follows from the continuity of tangential velocity across shock waves.

It should be remarked that there are other conservation forms which can be derived from the original equations. However integrated forms of these equations are not valid since the corresponding quantities are not conserved across

shock waves. For example, it follows from Eqs. (5) that

$$[(Ku^2 - v^2)/2 - (\gamma + 1)u^3/3]_x + (uv)_{\tilde{y}} = 0 \quad (15)$$

This form is connected to an over-all drag integral.[6]

In order to complete the specification of the problem the boundary conditions of tangent flow have to be written down. Within the first (and second) approximation the conditions may be applied in the plane of wing $\tilde{y} = 0$. The conditions are

$$\begin{aligned} \phi_{\tilde{y}}(x,0) &= F'(x), \quad |x| < 1 \\ &= 0, \qquad |x| > 1 \end{aligned} \quad (16)$$

where the body shape is given as $y = \delta F(x)$. The equations and boundary conditions set forth serve to define a presumably unique solution.

Solutions based on this theory in the transonic regime agree fairly well with experiment and with more exact theory. Spreiter[7] has shown that a choice of similarity parameter equivalent to

$$K_s = (1 - M_\infty^2)/(M^2\delta)^{2/3} \quad (17)$$

correlates the drag data for wedges very well. K is a similarity parameter in the sense that experiments on various affinely related bodies at different (M_∞,δ) scale in a known way for a given K. Some of the similarity rules based on the transonic expansion (with Spreiter's modification) are:
on body pressure coefficient

$$C_p(x) = (\delta/M_\infty)^{2/3}\bar{C}_p(x;K_s) \quad (18)$$

drag coefficient $$C_D = (\delta^{5/3}/M_\infty^{2/3})\bar{C}_D(K_s) \quad (19)$$

where $\bar{C}_p$, $\bar{C}_D$ are universal functions for airfoils of a given shape function $F(x)$.

III Formulation of Boundary Value Problem

In setting out to do numerical work on the finite difference analogue to the problem just posed two additional kinds of information are useful. One is a knowledge of the kinds of singularities in $\phi(x,\tilde{y})$ that can occur for a typical problem and the second is some analytic representation of the far field. The behavior of $\phi(x,\tilde{y})$ near singular points is obtained from local solutions of Eq. (8) or the corresponding hodograph equations. For example, from the many solutions for wedges[8,9] it is known that the pressure has a log singularity near the tip

$$\phi \sim x \log(x) \quad (20)$$

Also, it can be shown[6] that near a nose with a finite radius of curvature $C_p \sim x^{-1/3}$ or

$$\phi \sim x^{2/3} \quad (21)$$

For some of the examples calculated here a singularity of the type Eq. (20) occurs but this is sufficiently weak that it is ignored in the numerical work.

A more delicate region is the subsonic point just downstream of a shock where it strikes a curved surface. It is well known that the shock, normal to the surface at the wall, must have an infinite curvature there. Oswatitsch and Zierep[10] have provided a local solution which shows that downstream of the shock there is a rapid expansion of the flow followed by a smooth compression. Unfortunately the scale of this phenomenon is not determined by local considerations. Their formula is essentially

$$\phi = u^{(2)}(x - x_s) + f_{21}(\beta)r^2 \log r + f_{20}(\beta)r^2 + f_{32}(\beta)r^3 \log^2 r + \cdots$$

where $r^2 = (x - x_s)^2 + K\tilde{y}^2$, $\beta = \tan^{-1}(K\tilde{y}/x)$. f_{21}, etc., are known functions of β, except for one arbitrary constant. The occurrence of this singularity may affect the numerical results; again no explicit attempt was made to take it into account.

The other important information, the far field, is obtained by regarding Eq. (8) as an elliptic equation with a nonlinear right-hand side

$$L\phi \equiv K\phi_{xx} + \phi_{\tilde{y}\tilde{y}} = [(\gamma + 1)/2](u^2)_x \quad (22)$$

A Green's formula can be constructed for L in the upper half plane allowing for a shock (or shocks) across which there are jumps in $u = \phi_x$, $v = \phi_{\tilde{y}}$. The auxiliary function $\psi(\xi,\eta)$ is assumed continuous with continuous first derivatives. For $\phi(\xi,\eta)$, $\psi(\xi,\eta)$ we have

$$\iint_{\tilde{y}>0} (\psi L\phi - \phi L\psi)d\xi d\eta = \int_{\text{shock}} \psi_s\{\langle v\rangle d\xi - K\langle u\rangle d\eta\} - \int_{-\infty}^{\infty} (\psi\phi_\eta - \phi\psi_\eta)_{\eta=0}d\xi \quad (23)$$

Now, defining $\psi(\xi,\eta;x,\tilde{y})$ to be the fundamental solution for the full plane,

$$L_{\xi,\eta}\psi = \delta(x - \xi)\delta(\tilde{y} - \eta), \quad \psi = S(\xi - x,\eta - \tilde{y}) \quad (24)$$

and ϕ to be the flow satisfying Eq. (22), Eq. (23) becomes

$$\phi(x,\tilde{y}) = \int_0^\infty d\eta \int_{-\infty}^{\infty} d\xi\psi \frac{\gamma + 1}{2}\frac{\partial u^2}{\partial \xi} + \int_{\text{shock}} \psi_s(K\langle u\rangle d\eta - \langle v\rangle d\xi) + \int_{-\infty}^{\infty} (\psi\phi_\eta - \phi\psi_\eta)_{\eta=0}d\xi$$

The first integral is integrated by parts, taking into account that u^2 jumps across the shock(s), to give

$$\phi(x,\tilde{y}) = -\iint_{\tilde{y}>0} [\gamma + (1/2)]u^2\psi_\xi d\xi d\eta + \int_{\text{shock}} \psi_s\{[K\langle u\rangle - [\gamma + (1/2)]\langle u^2\rangle]d\eta - \langle v\rangle d\xi\} + \int_{-\infty}^{\infty} (\psi\phi_\eta - \phi\psi_\eta)_{\eta=0}d\xi \quad (25)$$

The integral along the shock(s) in Eq. (25) drops out because of the shock jump conditions Eq. (11) so that the folllowing integral formula holds for $\tilde{y} > 0$

$$\phi(x,\tilde{y}) = -\iint_{\tilde{y}>0} \frac{\gamma + 1}{2} u^2\psi_\xi d\xi d\eta + \int_{-\infty}^{\infty} (\psi\phi_\eta - \phi\psi_\eta)_{\eta=0}d\xi \quad (26)$$

Now the boundary term involving ψ_η can be eliminated in the usual way by a process of reflection. Define a reflected fundamental solution $\psi^*(\xi,\eta)$ such that

$$L_{\xi,\eta}\psi^* = \delta(x - \xi)\delta(-\tilde{y} - \eta), \quad \psi^* = S(\xi - x,\eta + \tilde{y})$$

Then, applying Green's formula to the same domain $(\tilde{y} > 0)$, but with ψ replaced by ψ^*, we have, corresponding to Eq. (26)

$$0 = -\iint_{\tilde{y}>0} \frac{\gamma + 1}{2} u^2\psi_\xi^* d\xi d\eta + \int_{-\infty}^{\infty} (\psi^*\phi_\eta - \phi\psi_\eta^*)_{\eta=0}d\xi \quad (27)$$

Using $\psi^*(\xi,0) = \psi(\xi,0)$, $\psi_\eta^*(\xi,0) = -\psi_\eta(\xi,0)$, and $\phi_\eta(\xi,0) = F'(\xi)$ for $|\xi| < 1$, the addition of Eqs. (26) and (27) gives

$$\phi(x,\tilde{y}) = 2\int_{-1}^{+1} F'(\xi)\psi(\xi,0)d\xi - \frac{\gamma + 1}{2}\int_0^\infty d\eta \int_{-\infty}^{\infty} d\xi u^2(\xi,\eta)[\psi_\xi + \psi_\xi^*] \quad (28)$$

The first integral in Eq. (28) can be integrated by parts and the boundary terms drop out for a closed airfoil $(F(\pm 1) = 0)$. The symmetry of ψ, ψ^*, and u with respect to η can be used

in the double integral so that

$$\phi(x,\bar{y}) = -2\int_{-1}^{+1} F(\xi)\psi_\xi(\xi,0)d\xi - \frac{\gamma+1}{2}\iint_{-\infty}^{\infty} u^2(\xi,\eta)\psi_\xi(\xi,\eta)d\xi d\eta \quad (29)$$

Now the fundamental solution of Eq. (24) is easily obtained by a scale transformation from the solution of Laplace's equation

$$\psi = S(x-\xi,\bar{y}-\eta) = 1/(2\pi K^{1/2})\log[(x-\xi)^2 + K(\bar{y}-\eta)]^{1/2}$$

Using this fundamental solution in Eq. (29) we obtain the basic integral equation for this problem

$$\phi(x,\bar{y}) = \frac{1}{\pi K^{1/2}}\int_{-1}^{+1}\frac{x-\xi}{(x-\xi)^2+K\bar{y}^2}F(\xi)d\xi + \frac{\gamma+1}{2}\frac{1}{2\pi K^{1/2}}\iint_{-\infty}^{\infty}\frac{(x-\xi)}{(x-\xi)^2+K(\bar{y}-\eta)^2}u^2(\xi,\eta)d\xi d\eta \quad (30)$$

A similar formula[6] can be derived for the airfoil which has lift in addition to thickness. The far field of Eq. (30) is thus that of the usual doublet for a closed body

$$\phi(x,\bar{y}) \cong (1/2\pi K^{1/2})\mathfrak{D}x/(x^2 + K\bar{y}^2) + \ldots \quad (31)$$

where

$\mathfrak{D}$ = doublet strength =

$$2\int_{-1}^{1} F(\xi)d\xi + \frac{\gamma+1}{2}\iint_{-\infty}^{\infty} u^2 d\xi d\eta \quad (32)$$

The doublet strength consists of the usual term proportional to the airfoil volume and a nonlinear contribution, unknown in advance. In the numerical procedure $\mathfrak{D}$ has to be calculated as one of the unknowns of the problem. The same is true of circulation in the lifting case.

The boundary value problem just formulated is presented schematically in Fig. 2. In the next section, the numerical aspects of the problem are discussed.

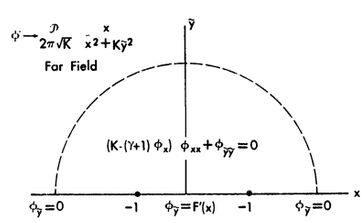

Fig. 2 Transonic boundary value problem.

IV Numerical Analysis

The transonic equation for the perturbation potential

$$[K-(\gamma+1)\phi_x]\phi_{xx} + \phi_{\bar{y}\bar{y}} = 0 \quad (33)$$

is a type of partial differential equation which has not been previously studied numerically. Standard references[11] on finite difference systems for partial differential equations point out the dissimilarities of such systems for purely elliptic and purely hyperbolic equations. These may be understood by considering the Laplace and wave equations shown in Fig. 3. For the Laplace equation, centered differences are used to approximate the derivatives. This properly accounts for the domain of dependence of the differential equation which extends in all directions. The x derivatives in the wave equation, however, must be approximated by one-sided differences to correctly represent the domain of dependence. For the explicit system, a restriction (the Courant-Fredrichs-Lewy criterion) on the step size in the x direction is needed to insure that the domain of dependence of the difference equation contains that of the differential equation. For the implicit system this is always true and there is no restriction on the step size. Thus the mathematical properties of the differential equation must be properly incorporated in the difference equation.

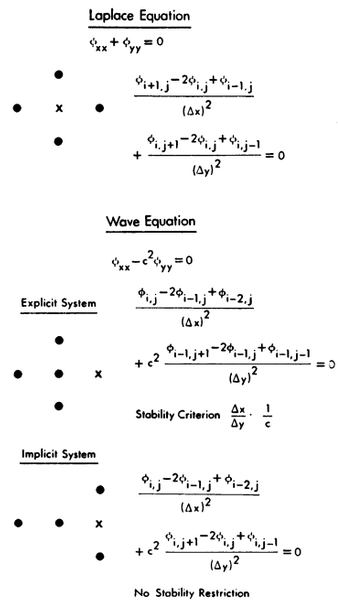

Fig. 3 Difference systems for the Laplace and wave equations.

A mixed difference system has been developed as the finite difference analogue of Eq. (33). To the authors' knowledge, the numerical procedure described in the following paragraphs constitute a new method of solving a mixed elliptic-hyperbolic differential equation. At each mesh point the velocity ϕ_x is computed and tested to determine if the flow is supersonic or subsonic. The appropriate hyperbolic (implicit) type or elliptic type difference equation is then selected for that mesh point. Thus the local domain of dependence of the differential equation is properly treated throughout the field. This procedure leads to a type sensitive difference system and a properly posed problem.

The resulting large set of simultaneous algebraic equations are solved in an iterative fashion using a line relaxation algorithm. Values of ϕ are solved for along a vertical (x = constant) line. Each vertical line is then successively relaxed proceeding in the positive x (time like) direction as discussed below. The latest values of ϕ are always used as they become available. At each stage of the iteration process, the local velocity is tested and the elliptic or hyperbolic difference system is selected. The sonic line and shock wave evolve naturally in the course of the iteration, and no guessing of their position is needed. The iteration is terminated when the solution converges to a final answer.

The difference formulas are derived from the transonic potential equation written in divergence form Eq. (7). The resulting formulas for the nonlinear term are as follows.

Elliptic System (2nd-Order Accurate)

$$\tfrac{1}{2}(\phi_x)_x^2 = [(\phi_{i+1}-\phi_i)^2 - (\phi_i-\phi_{i-1})^2]/2(\Delta x)^2$$

or when differentiated on the left and factored on the right

$$\phi_x\phi_{xx} = [(\phi_{i+1}-\phi_{i-1})/2\Delta x]\cdot[(\phi_{i+1}-2\phi_i+\phi_{i-1})/(\Delta x)^2] \quad (34)$$

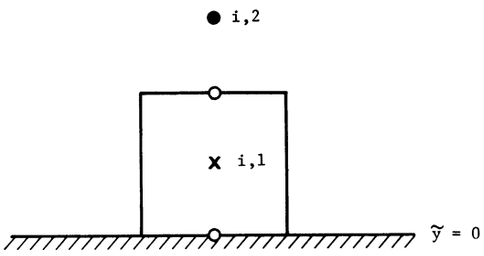

$$\phi_{\tilde{y}\tilde{y}} = \frac{1}{\Delta\tilde{y}}\left[\left(\phi_{\tilde{y}}\right)_{i,3/2} - \left(\phi_{\tilde{y}}\right)_{i,1/2}\right]$$

$$= \frac{1}{\Delta\tilde{y}}\left[\frac{\phi_{i,2} - \phi_{i,1}}{\Delta y} - \left(\phi_{\tilde{y}}\right)_{\tilde{y}=0}\right]$$

Fig. 4 Boundary condition for $\tilde{y} = 0$.

Hyperbolic System (1st-Order Accurate)

$$\tfrac{1}{2}(\phi_x)_x{}^2 = [(\phi_i - \phi_{i-1})^2 - (\phi_{i-1} - \phi_{i-2})^2]/2(\Delta x)^3$$

or

$$\phi_x\phi_{xx} = [(\phi_i - \phi_{i-2})/2\Delta x]\cdot[(\phi_i - 2_{i-1} + \phi_{i-2})/(\Delta x)^2] \quad (35)$$

Hyperbolic System (2nd-Order Accurate)

$$^1(\phi_x)_x{}^2 =$$

$$[(2\phi_i - 3\phi_{i-1} + \phi_{i-2})^2 - (2\phi_{i-1} - 3\phi_{i-2} + \phi_{i-3})^2]/2(\Delta x)^3$$

or

$$\phi_x\phi_{xx} = \frac{2\phi_i - \phi_{i-1} - 2\phi_{i-2} + \phi_{i-3}}{2\Delta x} \times \frac{2\phi_i - 5\phi_{i-1} + 4\phi_{i-2} - \phi_{i-3}}{(\Delta x)^2} \quad (36)$$

The linear ϕ_{xx} term corresponds to the second factor on the right-hand side of the above equations. Both of the implicit hyperbolic systems have been used as discussed in Section V. The usual centered formula for $\phi_{\tilde{y}\tilde{y}}$ is used everywhere except on the $\tilde{y} = 0$ boundary.

On the $\tilde{y} = 0$ axis the boundary condition to be applied is the value of $\phi_{\tilde{y}}$ (Fig. 2). The boundary is placed along the edge of the mesh cell and $\phi_{\tilde{y}\tilde{y}}$ is written as in Fig. 4. This is a consistent method of treating the boundary condition and leads to a tridiagonal matrix of the values of ϕ along a vertical line. The accuracy of the method was confirmed by comparing an exact and numerical solution of the Laplace equation with boundary conditions corresponding to a circular arc airfoil. The final values of ϕ at $\tilde{y} = 0$ which are needed to calculate surface pressures, etc., are obtained using a second-order accurate extrapolation formula.

In the far field, ϕ is specified on the boundary mesh points according to Eq. (31). The area integral of $\phi_x{}^2$ needed for the far field boundary condition is calculated using the trapezoidal rule. Contributions to the integral from outside the far field boundaries are negligible. The integral must be periodically recalculated as the computation proceeds.

The simultaneous algebraic equations are solved by line relaxation. We define

$$\Phi_i = \begin{pmatrix} \phi_{i,1} \\ \cdot \\ \cdot \\ \cdot \\ \phi_{i,J} \end{pmatrix} \quad (37)$$

as a J dimensional column vector whose elements are the values of ϕ on a vertical line. Then the line relaxation formula takes the form

$$\Phi_i{}^{n+1} = \omega\hat{\Phi}_i{}^{n+1} + (1 - \omega)\Phi_i{}^n \quad (38)$$

where $\hat{\Phi}_i{}^{n+1}$ is the solution of the simultaneous equations along the i = constant line. The parameter n represents the number of iterations through the entire field, and ω is a relaxation parameter which was usually between 0.9 and 1.0. The iterations diverged for $\omega > 1$ if there are supersonic points in the field. The iterations are performed by successively relaxing the vertical lines, sweeping the field from left to right. This order in which the lines are relaxed is implied in the hyperbolic difference equations as they are written (Eqs. (35) and (36)). Basically, this is due to the fact that information is propagated through the supersonic flow from left to right along the characteristic directions [Eq. (9)].

If a vertical line contains only elliptic points the J simultaneous equations for the elements of $\hat{\Phi}_1{}^{n+1}$ are linear and may be written as

$$A\hat{\Phi}_i{}^{n+1} = f \quad (39)$$

A is a $J \times J$ dimensional tridiagonal matrix (diagonally dominant). The components of the J dimensional column vector f consist of values of ϕ at $i + 1$, $i - 1$, and $i - 2$ (for hyperbolic points). Equations (39) may be solved by direct elimination. If a vertical line contains any hyperbolic points the J simultaneous equations for $\hat{\Phi}_i{}^{n+1}$ are nonlinear. Various methods are available to solve such systems, but the one used here consists of writing the system in the form of Eq. (39) where A and f are then functions of $\hat{\Phi}_i{}^{n+1}$. The set may be solved by the simple iteration procedure

$$A(\hat{\Phi}_i{}^{n+1,\nu})\hat{\Phi}_i{}^{n+1,\nu+1} = f(\hat{\Phi}_i{}^{n+1,\nu}) \quad (40)$$

which usually converged in 2 to 3 iterations. This equation may be over or under relaxed also.‡

Various difference formulas exist which can be used to compute the local velocity to test for subsonic or supersonic flow. Since derivatives of ϕ are discontinuous at the shock wave, not all formulas give the same result. Numerical experimentation was carried out to determine the proper difference formula. It was found that the centered formula

$$\phi_{x_{\text{test}}} = (\phi_{i+1} - \phi_{i-1})/2\Delta x \quad (41)$$

was best. This formula was also used to compute the final output. Thus ϕ_x was calculated with the centered difference everywhere except in the hyperbolic difference system where Eqs. (35) or (36) were used.

The initial guess $\phi_i{}^0$ was obtained from the final values of a previous calculation. A subcritical solution was first computed and then solutions for decreasing K were computed in succession. Absolute convergence was established by computing answers at several values of K with initial guesses from "above" and "below."

The shock wave, if present, develops naturally in the course of the iterations. No artificial viscosity was added to produce the shock structure. Apparently there is sufficient dissipation within the difference equations and relaxation algorithm to produce a shock wave spread over 3–4 mesh points. The properties of the ordinary differential equation corresponding to x derivatives of Eq. (33) and the lowest order truncation errors of Eqs. (34) to (36) were studied. Only the differential equation corresponding to (36) provides a shock wave like structure as a solution. Work is being done to understand the origin of the dissipation in the solution.

For the results reported below there are 74 mesh points along the x axis and 41 along the $\tilde{y}$ axis (except for the few cases mentioned with 148 points along the x axis). In the x direction the mesh points were spaced evenly over the air-

‡ Subsequent to the work reported here, this method for solving the nonlinear equations has been replaced by Newton's method at the suggestion of H. Keller.

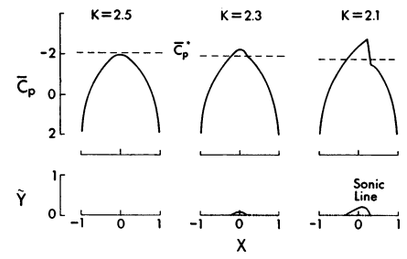

Fig. 5 Pressure distributions and sonic line locations for circular arc airfoil. Transition from subcritical to supercritical flow.

foil (40 total). Fore and aft of the airfoil a stretched coordinate ξ was used where

$$\xi + d = (x + c)^{-1}$$

Similarly a stretch coordinate η was used in the y direction

$$\eta + b = (\tilde{y} + a)^{-1}$$

The constants a,b,c,d were conveniently chosen, and the boundaries of the mesh network were at $x \simeq \pm 5.6$, $\tilde{y} = 0$, $\tilde{y} = 7.5/K^{1/2}$. This inverse coordinate stretching was motivated by the far field behavior of ϕ (Eq. (31)). Computations were done on an IBM 360/44. A typical calculation took about 400 iterations with a corresponding computing time of about 30 minutes. The same computation will be faster on the CDC 6600 by better than one order of magnitude.

V Results

Computations have been performed for circular arc airfoils and a Nieuwland airfoil (NLR 0.120–0.700–0.000). Circular arc airfoils have been studied previously, both analytically and experimentally, and hence serve as a good model to test the present theory. The equation for the airfoil is $y = \delta(1 - x^2)$.

Plots of the pressure coefficient and sonic line position over the circular arc airfoil are shown in Figs. 5 and 6 for various values of K. Figure 5 shows the transition from completely subcritical flow to a supercritical flow with an imbedded shock wave. For subcritical values of K ($K_{crit} \simeq 2.45$) the pressure distribution is symmetric about $x = 0$. The solutions quickly become asymmetric as K decreases and supercritical velocities are reached. For a limited range of K a small shock-free supersonic region is found. As K becomes progressively smaller (Fig. 6), the supersonic zone grows and the shock wave strengthens and moves rearward on the airfoil. At the same time the downstream boundary of the supersonic region steepens up to become more vertical.

In Fig. 7 calculated results are compared with the experimental data of Knechtel[12] for a subcritical case and a supercritical flow with an imbedded shock wave. Spreiter's relations for K_s and $\tilde{C}_p$ (Eqs. 17 and 18) were used to reduce

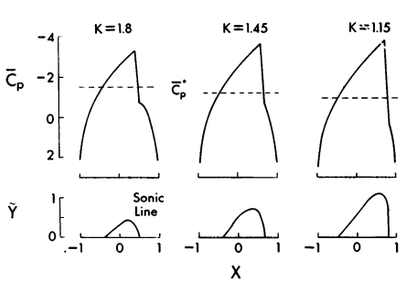

Fig. 6 Pressure distributions and sonic line locations for circular arc airfoil.

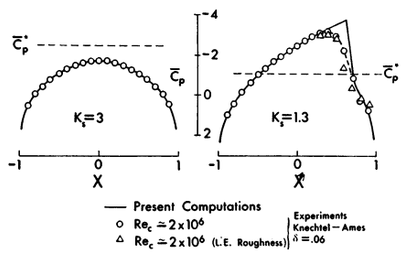

Fig. 7 Pressure distributions for circular arc airfoil. Comparison between experimental and computed results.

Knechtel's data to transonic similarity form. Agreement between theory and experiment is excellent for the subcritical case. For the supercritical example the agreement upstream and downstream of the shock wave is excellent. Near the shock-wave the experiment and theory deviate, most probably as a result of shock wave-boundary layer interaction in the experiments. The boundary layer in the experiments was laminar and hence would be subject to extensive interaction effects. Knechtel conducted some tests with roughness elements added near the leading edge and those results are also shown in Fig. 7. The location of the shock wave and the pressure rise across it are adequately predicted by the theory.

It is well known that there must be a singularity in the inviscid solution where a supersonic to subsonic shock wave is incident on a curved wall (see Sec. III). The solution by Oswatitsch and Zierep[10] predicts that a rapid expansion followed by a smooth compression along the surface will occur downstream of the shock wave incident on a convex body. Measurements by Ackeret, Feldman, and Rot[13] show that such a structure is found for a shock wave above a curved plate. A portion of their measurements are reproduced in Fig. 8. On the plate surface the shock wave pressure rise is smeared out by the turbulent boundary layer over several boundary-layer thicknesses ($\delta \simeq 5$mm). However, outside the boundary layer the expansion is evident. Its strength decays with increasing distance above the plate. At $y = 15$ mm and 45 mm the full pressure rise for a normal (or nearly normal) shock is not measured. At $y = 75$ mm the measured pressure increase is greater than the normal shock value.

Calculated pressure and flow angularity distributions in the neighborhood of the shock wave above the circular arc airfoil are shown in Fig. 9. The jumps in u and v may be estimated from these results and the shock polar and angle [Eqs. (11) and (12)] may be computed. At $\tilde{y} = 0$ the full pressure rise for a normal shock is not realized. Apparently the calculations smooth out the rapid expansion predicted by the Oswatitsch and Zierep solution. The calculated results are typical of measured surface pressure data. The shock wave weakens with increasing distance above the airfoil surface and, for this value of K, bends upstream and becomes oblique. Below $\tilde{y} \simeq 0.179$ the jumps in (u,v) do not satisfy

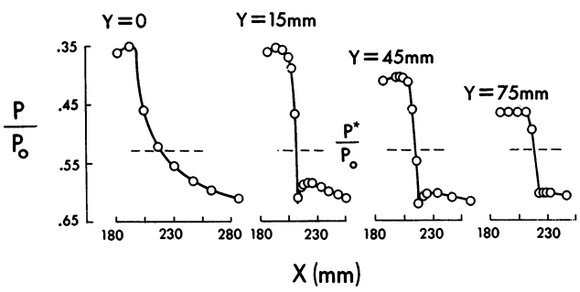

Fig. 8 Measured static pressure distribution through a shock wave at various distances above a curved plate: experiments of Ackeret, Feldman, and Rot.[13]

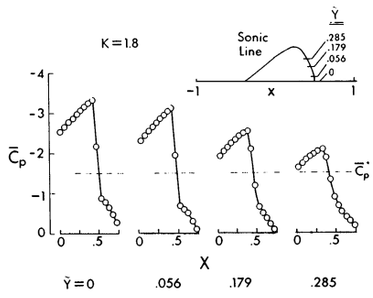

Fig. 9a Computed pressure distribution through a shock wave at various distances above a circular arc airfoil.

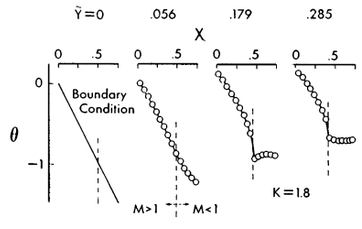

Fig. 9b Computed flow angularity distribution through the shock wave at various distances above a circular arc airfoil.

the shock polar equation due to the influence of the singularity. Above $\bar{y} \simeq 0.179$ the agreement with the shock polar is good. The calculated pressure profiles (Fig. 9a) agree qualitatively with Ackeret, Feldman and Rot's data where again the finite difference calculations appear to have smoothed out the measured expansion region following the shock. From Fig. 8, the extent of this region is about 0.01 times x, the distance from the leading edge. In the present computations the mesh spacing Δx is 0.025 times the airfoil chord. Presumably a refined mesh near the shock wave would allow the expansion region to be computed. In both Ackeret's experiments and the present calculations, the influence of the singularity at the wall extends outward for a considerable distance.

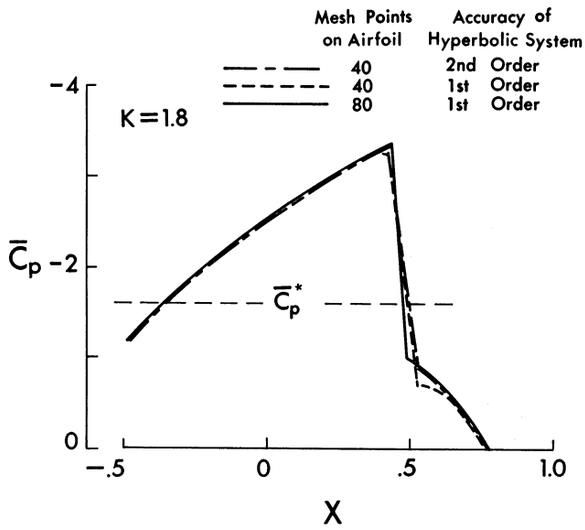

Fig. 10 Comparison of computed results using first and second order accurate hyperbolic difference systems and twice the number of mesh points in the x direction.

Computations were done using both the first- and second-order accurate hyperbolic systems [Eqs. (35) and (36)]. A typical comparison is shown in Fig. 10. Also shown is a result computed with twice the usual number mesh points in the x direction (148 total, 80 on the airfoil). The only noticeable differences over the whole field are confined to two or three mesh points downstream of the shock wave. All three computations predict the same shock wave location. The first-order accurate hyperbolic system is recommended for general use. The four point second-order system can be quite inaccurate in situations where ϕ_x changes rapidly in the supersonic region.

The present computational techniques have been used to calculate the flow about a Nieuwland airfoil. These airfoil shapes are obtained using hodograph methods and thus represent exact solutions of the full inviscid equations. Hodograph techniques may be used to calculate shock-free flows with imbedded shock waves. Nieuwland[1] has reported results for shock-free flows about a series of quasi-elliptical airfoil shapes. One of these NLR 0.12–0.70-0.00 was selected which has a doubly symmetric profile similar to a circular arc airfoil. The airfoil has a thickness ratio of 10.76% and the shock-free solution occurs at $M_\infty = 0.8257$.

Computed results of pressure coefficient and sonic line position are compared with the exact solution in Fig. 11. The agreement is excellent. The exact solution of the full inviscid equations is symmetric about the airfoil midchord. Such a shock-free solution relies on a delicate interaction of expansion and compression waves with each other and the airfoil surface to yield a smooth recompression. The finite difference solution of the small disturbance equations show some slight asymmetry with a weak expansion near the terminus of the supersonic zone. This small difference is not surprising since the equations are an approximate version of the full equations, the boundary conditions are applied on $y = 0$ axis rather than the airfoil surface, and the airfoil slope at the desired mesh points were obtained by interpolation from the given values.[14] Additional calculations have been done using slightly different interpolated values (maximum difference of 1% in airfoil slope) and double the number of mesh points. Results are essentially the same as those shown with small differences at the terminus of the supersonic zone. It should be noted that the results in Fig. 11 are presented in physical coordinates rather than transonic ones. This is a good test of the accuracy of the transonic scaling rules.

The computations for the Nieuwland airfoil were done starting with a subcritical case and calculating cases for successively lower values of K. Thus, the "design point" solution of Fig. 11 was imbedded in a family of "off-design" solutions. Figure 12 shows three cases, one of which is the shock-free solution discussed above. The off-design solutions are quite asymmetric. For $K = 1.82$ there are two compression regions on the airfoil surface. The first compression zone is smooth and no shocks build up. The second compression may be a weak shock, but it is difficult to tell from the

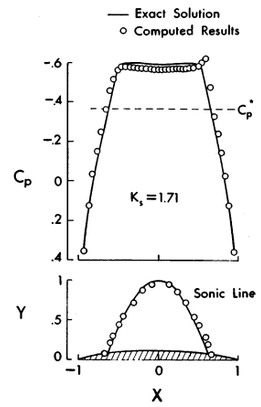

Fig. 11 Comparison of exact theory and computed results for a Nieuwland airfoil (NLR 0.12-0.70-0.00).

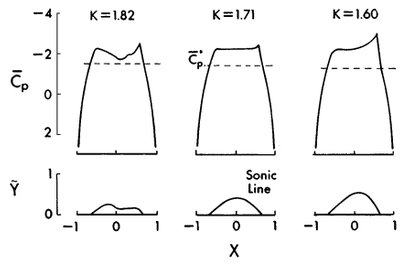

Fig. 12 Computed pressure distributions and sonic line locations for three values of K for a Nieuwland airfoil (NLR 0.12-0.70-0.00).

present calculations due to the steep pressure gradients on the aft section of the airfoil. At $K = 1.60$ a weak shock wave terminates the supersonic zone.

As was discussed in Sec. II, the formula for K is not uniquely defined by the systematic expansion procedure. For the Nieuwland airfoil at design conditions ($\delta = 0.0176$, $M_\infty = 0.8257$) the values of K corresponding to Eqs. (1) and (17) are 1.41 and 1.82, respectively. A definition of K which corresponds closely to 1.71 is $(1 - M_\infty^2)/M_\infty\delta^{2/3}$. However, it cannot be concluded on the basis of one calculation that this is a more accurate formula in general. Finally it is worth noting that for $\delta = 10.76\%$ the increments of K in Fig. 12 correspond to increments in M_∞ on the order of 0.01.

VI Summary

Small disturbance theory has been used to investigate steady transonic flow past thin airfoils. The governing nonlinear transonic equation for the perturbation potential contains the essential features of this mixed subsonic-supersonic flow with imbedded shock waves. A boundary value problem was formulated and an analytical solution derived for the far field. For the near field a mixed finite difference system was developed to solve the transonic equation. The local elliptic or hyperbolic nature of the equation is explicitly taken into account by the finite difference equations to give a properly posed problem. The equations are then solved by an iterative relaxation algorithm which converges well. The supersonic zone and shock waves appear naturally in the course of the solution. This newly developed mixed finite difference system could have application to other problems involving mixed elliptic-hyperbolic differential equations.

Results have been computed for circular arc airfoils and a Nieuwland airfoil for several values of K, the transonic similarity parameter. For the circular arc airfoil the results have been compared with wind tunnel experiments and the agreement is excellent. The shock wave region above the airfoil has been qualitatively compared with the measurements of Ackeret, Feldmann and Rott[13] and agreement is apparent. For the Nieuwland airfoil the computed results and exact theory show excellent agreement for the design point solution. Several off-design results obtained with the present method are also presented.

The small disturbance formulation of the transonic problem appears to be quite accurate. The ability to extend it to lifting problems and three dimensional flows is a definite asset, and this course is being pursued. The numerical procedures developed for the nonlifting airfoil studies are rapid and accurate. The computational methods hold the promise of being a useful tool for wing design applications, thereby reducing the extensive experimental work now required.

References

[1] Nieuwland, G. Y., "Transonic Potential Flow around a Family of Quasielliptical Aerofoil Sections," TR T.172, 1967, National Lucht-en Ruimtevaartlaboratorium, The Netherlands.

[2] Korn, D. G., "Computation of Shock-free Transonic Flows for Airfoil Design," NYO-1480-125, Oct. 1969, Courant Institute of Mathematical Sciences, New York University, New York.

[3] Magnus, R. and Yoshihara, H., "Inviscid Transonic Flow over Airfoils," AIAA Paper 70-47, New York, Jan. 1970.

[4] Cole, J. D. and Messiter, A. F., "Expansion Procedures and Similarity Laws for Transonic Flow," *Zeitschrift für angewandte Mathematik und Physik*, Vol. 8, No. 1, 1957, pp. 1–25.

[5] Hayes, W. D., "La seconde approximation pour les écoulements transoniques non visqueux," *Journal de Mecanique*, Vol. 5, No. 2, June 1966, pp. 163–206.

[6] Cole, J. D., "Twenty Years of Transonic Flow," Document D1-82-0878, July 1969, Boeing Scientific Research Laboratories, Seattle, Wash.

[7] Spreiter, J., "On the Application of Transonic Similarity Rules to Wings of Finite Span," TR 1153, 1953, National Advisory Committee for Aeronautics.

[8] Cole, J. D., "Drag of Finite Wedge at High Subsonic Speeds," *Journal of Mathematics and Physics*, Vol. 30, No. 2, July 1951, pp. 79–93.

[9] Guderley, G. and Yoshihara, H., "The Flow Over a Wedge Profile at Mach Number 1," *Journal of the Aeronautical Sciences*, Vol. 17, No. 11, Nov. 1950, pp. 723–735.

[10] Oswatitsch, K. and Zierep, J., "Das Problem des senkrechten Stosses an einer gekrümmten Wand," *Zeitschrift fur angewandte Mathematik und Mechanik*, Vol. 40, Supplement, 1960, pp. T143–T144.

[11] Isaacson, E. and Keller, H. B., *Analysis of Numerical Methods*, Wiley, New York, 1966.

[12] Knechtel, Earl D., "Experimental Investigation at Transonic Speeds of Pressure Distributions over Wedge and Circular-Arc Airfoil Sections and Evaluation of Perforated-Wall Interference," TN D-15, 1959, NASA.

[13] Ackeret, J., Feldman, F., and Rott, N., "Investigation of Compression Shocks and Boundary Layers in Gases Moving at High Speeds," TM 1113, 1947, National Advisory Committee for Aeronautics, Translated from ETH, Zurich Rept. 10, 1946.

[14] Baurdoux, H. I. and Boerstoel, J. W., "Symmetrical Transonic Potential Flows Around Quasi-elliptical Aerofoil Sections," NLR-TR 69007U, Dec. 1968, National Lucht-En Ruimteraart-Rept. laboratorium, The Netherlands.